Electronic Supplementary Material (ESI) for Nanoscale Advances.

Supplementary Material

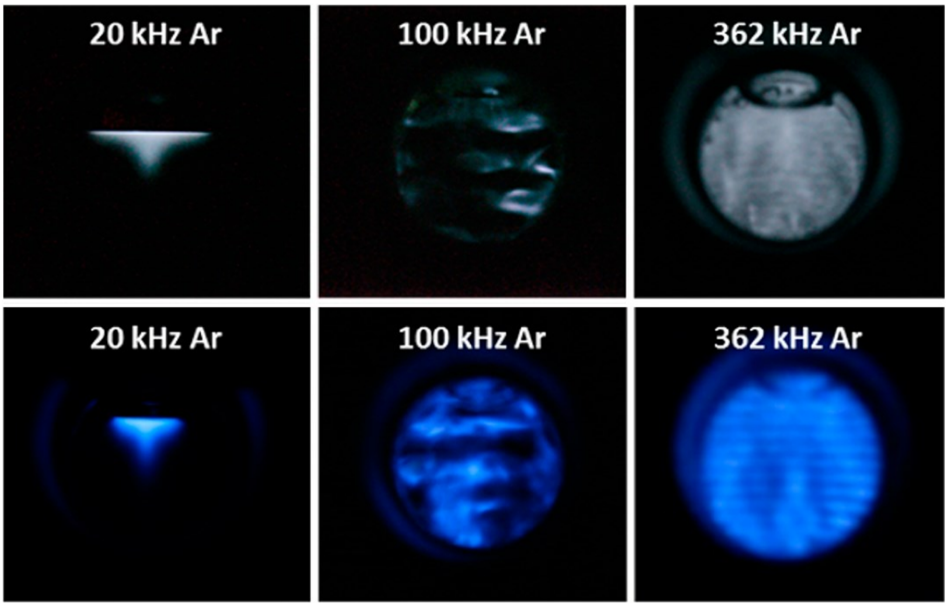

Figure S1. Photographs of sonochemiluminescence: Upper photographs in water at 20 kHz (P_{ac} = 33 W), 100 kHz (P_{ac} = 40 W), and 362 kHz (P_{ac} = 43 W) under 100 mL•min^{-1} Ar flow, at 18 ℃, exposure time of camera was 60 s; Below photographs in 0.01 M luminol solution (pH 11, Na_2CO_3) at 20 kHz (P_{ac} = 33 W), 100 kHz (P_{ac} = 40 W), and 362 kHz (P_{ac} = 43 W) under 100 mL•min^{-1} Ar flow, at 18 ℃, exposure time of the camera was 10 s. Reproduced with permission from ref. [31]. Copyright 2018 American Chemical Society.

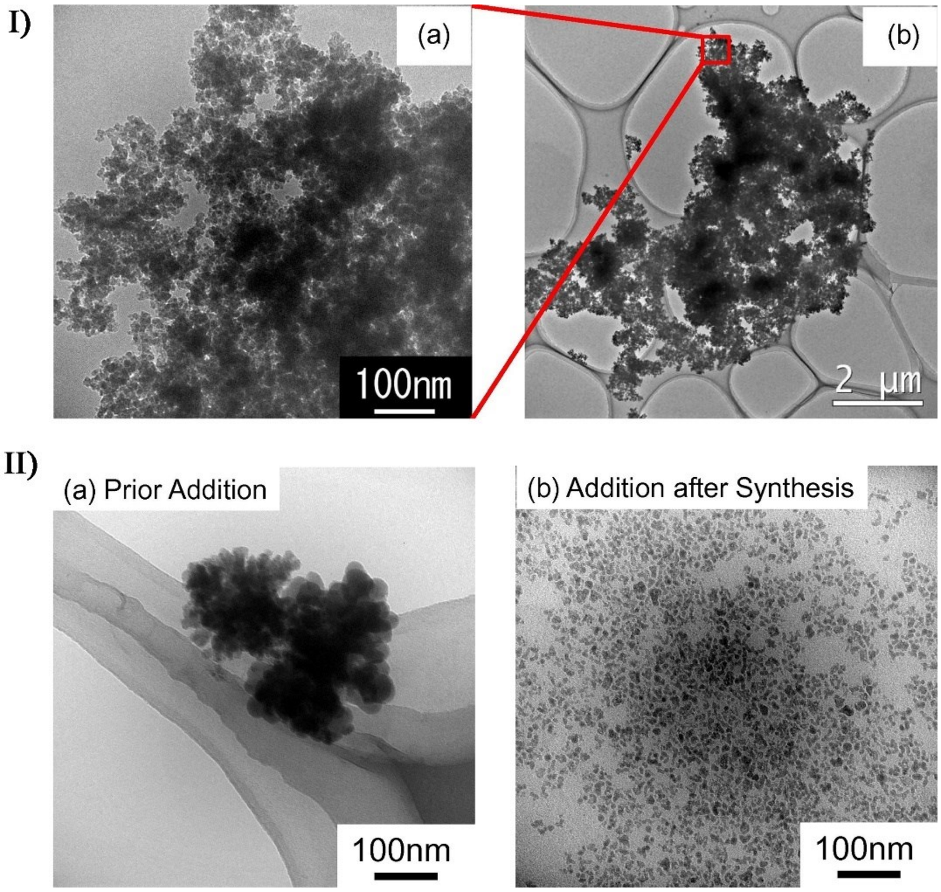

Figure S2. I) TEM images of ultrasonic-derived product without the addition of surfactant (a, b), where the scale bars were 100 nm in (a) and 2 μm in (b); II) TEM images of ultrasonic-derived product: addition of surfactant before (a) and after (b) the sonochemical synthesis, where the scale bars were 100 nm. Reproduced with permission from ref. [42]. Copyright 2017 Elsevier.

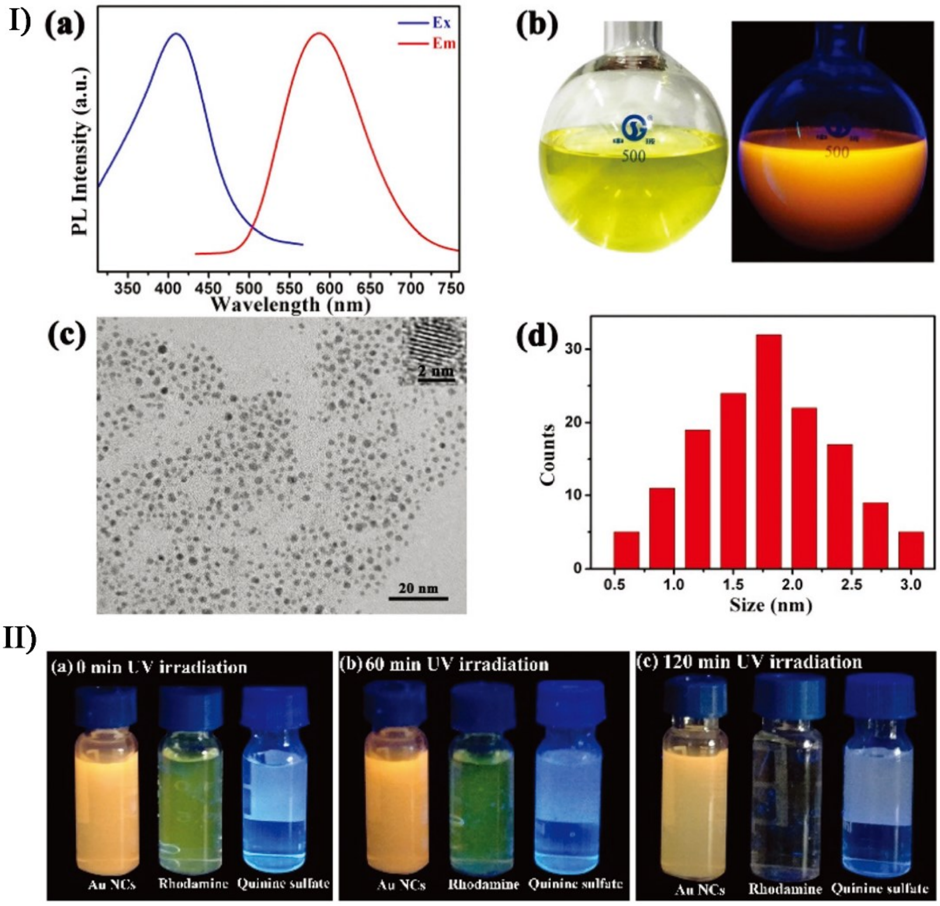

Figure S3. I) Excitation (E_x) and emission (E_m) spectra of Au nanoclusters (Au NCs) (a), Photographs of Au NCs under visible (Left) and 365 nm UV (Right) light (b), TEM and HRTEM (inset) image of Au NCs (c), and Size distribution of Au NCs (d), average size = 1.7 ± 0.3 nm, where the scale bars were 20 nm in (c) and 2 nm (inset); II) Photographs of Au NCs, rhodamine and quinine sulfate aqueous solutions under UV irradiation for different time periods (a, b, and c), where all samples were continuously irradiated by a 500 W xenon lamp. Reproduced with permission from ref. [56]. Copyright 2018 Royal Society of Chemistry.

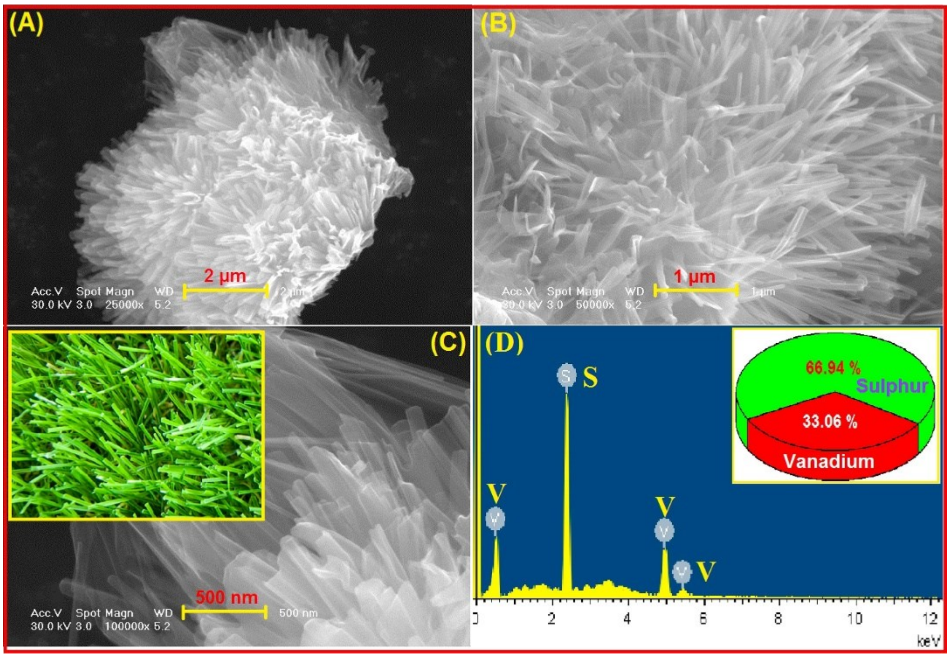

Figure S4. FESEM micrographs (A-C) of grass-like VS_2 with different magnifications, where the scale bars were 2 µm in (A), 1 µm in (B) and 500 nm in (C); EDX spectrum of grass-like VS_2 (D), where the inset was EDX quantitative analysis. Reproduced with permission from ref. [100]. Copyright 2018 Elsevier.

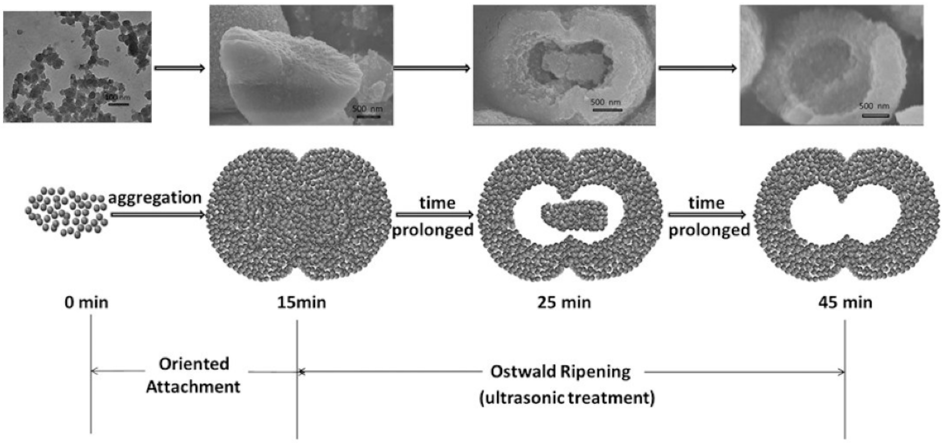

Figure S5. Schematic formation process based on the oriented attachment and Ostwald ripening mechanism, where the scale bars were 100 nm (first image) and 500 nm (other images). Reproduced with permission from ref. [111]. Copyright 2015 Royal Society of Chemistry.

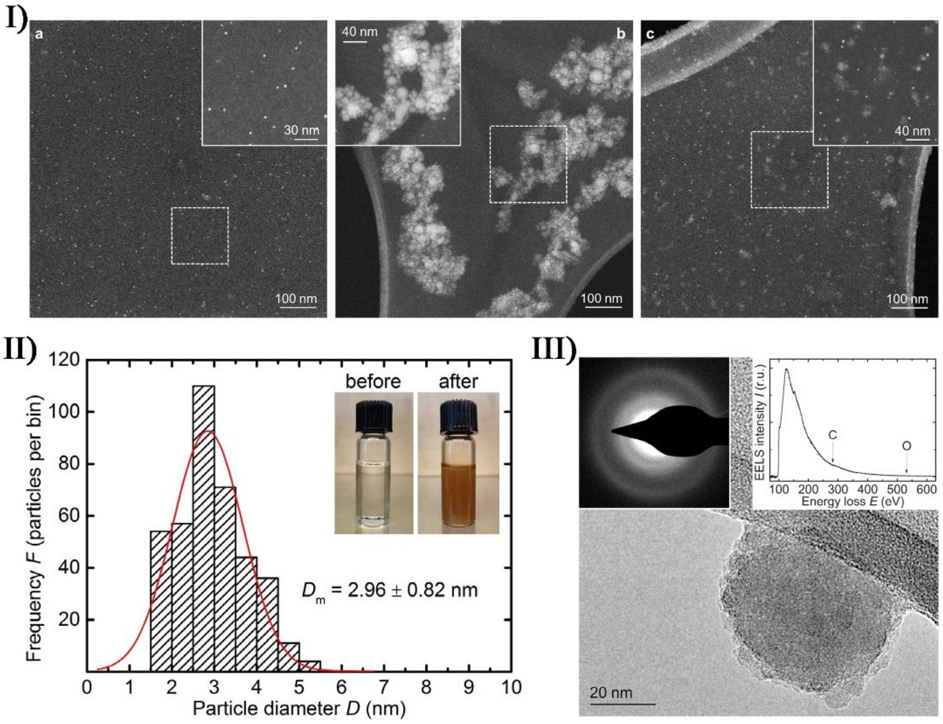

Figure S6. I) Dark field STEM images (scale bars = 100 nm) depicting the effects of sonication conditions on Si-nanoparticle production: (a) Monodisperse Si-nanoparticles synthesized with low tip amplitude (A = 48 μm) and high-concentration Si_3H_8 (47 wt%), (b) larger Si-nanoparticles synthesized with both high A (192 μm) and high-concentration Si_3H_8, and (c) blend of Si-nanoparticles synthesized with high A and low-concentration Si_3H_8 (1 wt%). The insets showed higher resolution images (a: scale bars = 30 nm; b and c: scale bars = 40 nm) of the regions enclosed by the dashed boxes. II) Histogram of the 387 particles in I-a with a Gaussian fit to the data in red. The photographs in the inset showed a glass vial containing a solution before and after sonication for ~45 min. III) Bright field TEM image (scale bar = 20 nm) of a~50 nm cauliflower-like S Si-nanoparticles (A = 192 μm, Si_3H_8 concentration =47 wt%) attached to the rim of the C grid. The electron diffraction pattern showed a set of diffuse rings demonstrating the amorphous nature of the particle. The core-level EELS spectrum showed the Si $L_{2,3}$-edge at~100 eV. The slight elevation at ~280 eV (C) was the carbon K-edge and no trace of the oxygen K-edge (O) was evident at ~530 eV. Reproduced with permission from ref. [146]. Copyright 2017 Elsevier.

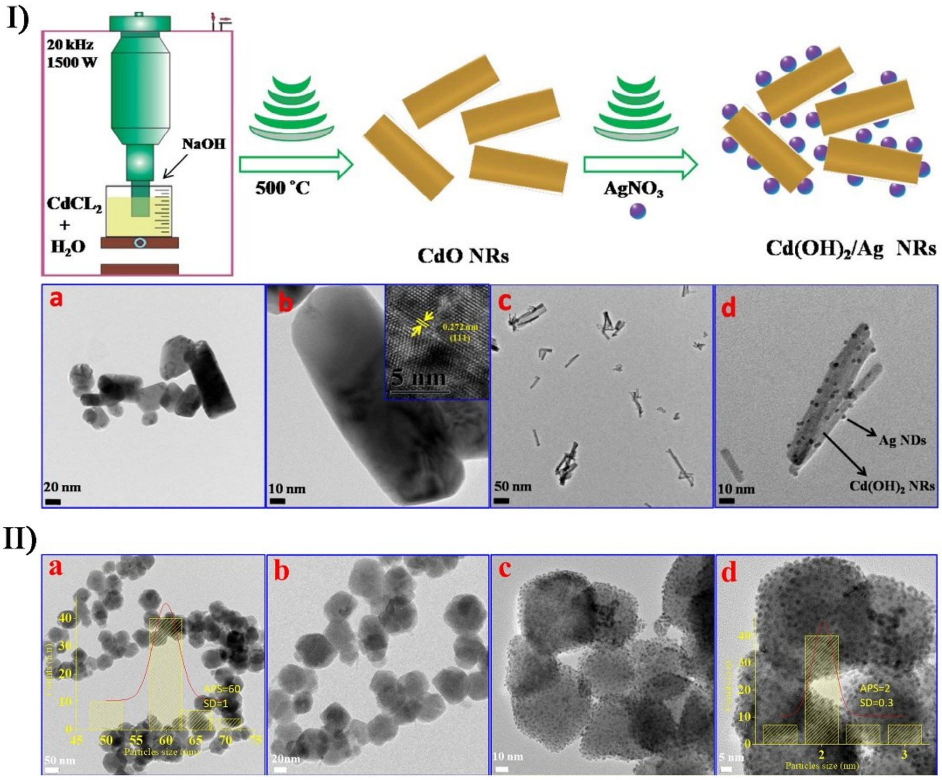

Figure S7. I) schematic overview the general mechanism and main steps for the synthesis of CdO and Cd(OH)$_2$/Ag core/satellite nanorods. TEM images of CdO nanorods (a: scale bar = 20 nm; b: scale bar = 10 nm) and Cd(OH)$_2$/Ag nanorods (c: scale bar = 5 nm; d: scale bar = 10 nm), where the inset was the HRTEM image (scale bars = 5 nm) of CdO nanorods in Image b. Reproduced with permission from ref. [153]. Copyright 2018 Elsevier. II) TEM micrographs of (a: scale bar = 50 nm; b: scale bar = 20 nm) Fe$_2$O$_3$/ZrO$_2$ nanocubes and (c: scale bar = 10 nm; d: scale bar = 5 nm) Au-decorated Fe$_2$O$_3$/ZrO$_2$ nanocubes. Reproduced with permission from ref. [154]. Copyright 2019 Elsevier.

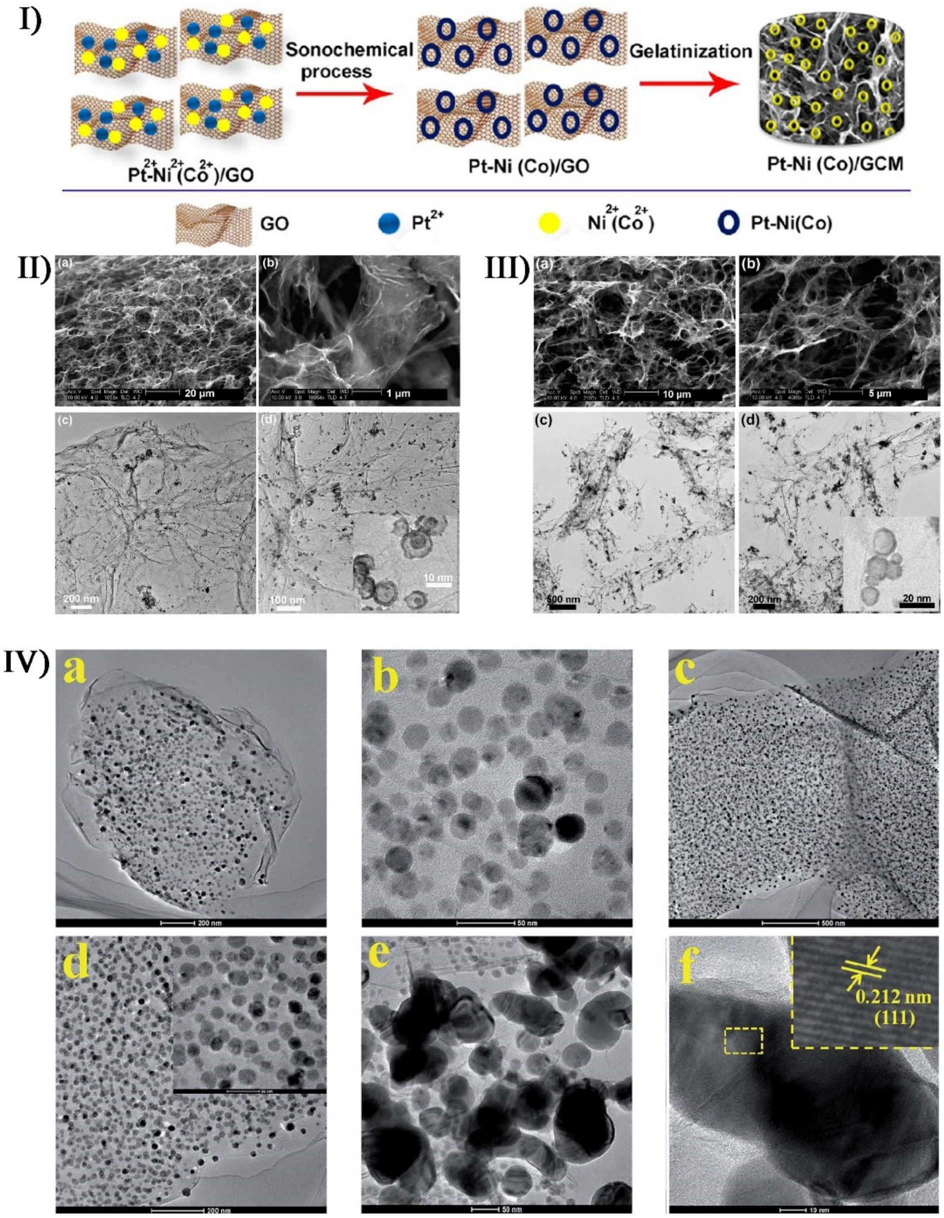

Figure S8. I) Schematic illustration of the synthesis procedure of hollow Pt-M/GCM (M = Ni, Co) porous electrocatalysts; II) Morphology and structure characterization of Pt-Ni/GCM: SEM images (a: scale bar = 20 μm; b: scale bar = 1 μm), and TEM images (c: scale bar = 200 nm; d: scale bar = 100 nm); III) Morphology and structure characterization of Pt-Co/GCM: SEM images (a: scale bar = 10 μm; b: scale bar = 5 μm), and TEM images (c: scale bar = 500 nm; d: scale bar = 200 nm). Reproduced with permission from ref. [170]. Copyright 2016 American Chemical Society. IV) TEM images for the spent ultrasound-synthesized Cu/RGO catalysts in the presence of ammonia: 10 wt% (a: scale bar = 200 nm; b: scale bar = 50 nm), 25 wt% (c: scale bar = 500 nm; d: scale bar = 200 nm), and 45 wt% (e: scale bar = 50 nm; f: scale bar = 10 nm). Reproduced with permission from ref. [171]. Copyright 2018 Royal Society of Chemistry.

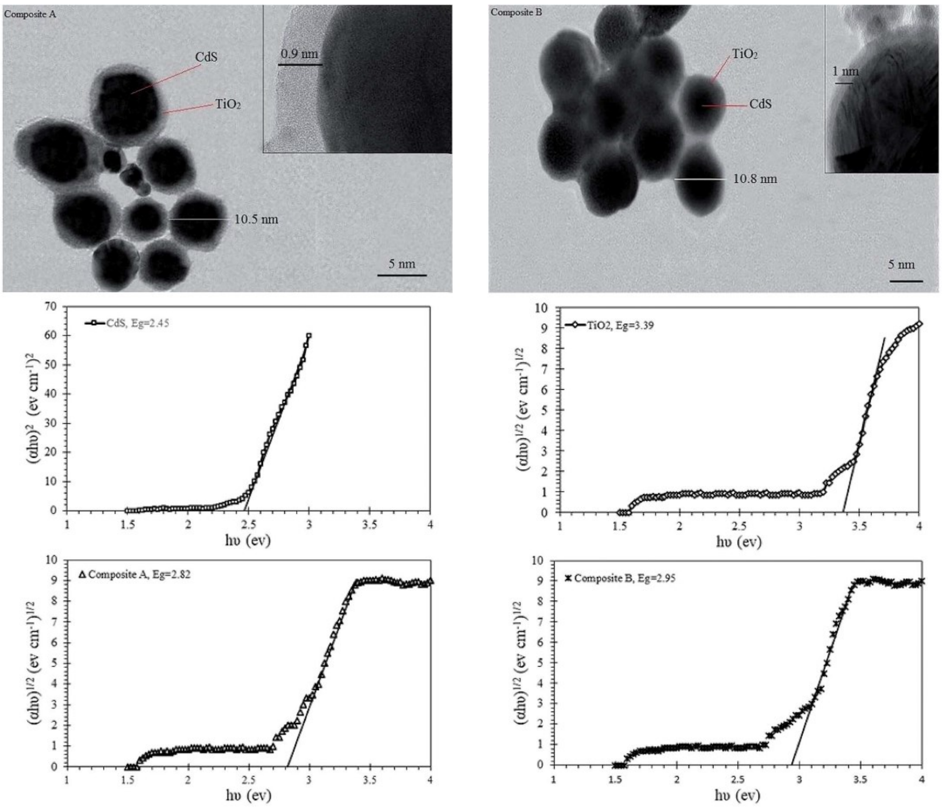

Figure S9. Top: TEM images (scale bars = 5 nm) of CdS/TiO_2 nanocomposites, where the TiO_2/CdS molar ratio for composite A and composite B were 2.97 and 4.87, respectively. Below: Band gap of pure CdS, pure TiO_2, composite A and composite B. Reproduced with permission from ref. [177]. Copyright 2019 Royal Society of Chemistry.